Staging Liver Fibrosis by Fibroblast Activation Protein Inhibitor PET in a Human-Sized Swine Model

Ali Pirasteh[1], Sarvesh Periyasamy[2], Jennifer Jean Meudt[3], Yongjun Liu[4], Laura M. Lee[5], Kyle M. Schachtschneider[6,7], Lawrence B. Schook[8,9], Ron C. Gaba[9], Lu Mao[10], Adnan Said[11,12], Alan Blair McMillan[1], Paul F. Laeseke[2], and Dhanansayan Shanmuganayagam[3,13,14]

[1]Radiology and Medical Physics, University of Wisconsin–Madison, Madison, Wisconsin; [2]Radiology and Biomedical Engineering, University of Wisconsin–Madison, Madison, Wisconsin; [3]Animal and Dairy Sciences, University of Wisconsin–Madison, Madison, Wisconsin; [4]Pathology and Laboratory Medicine, University of Wisconsin–Madison, Madison, Wisconsin; [5]Research Animal Resources and Compliance, University of Wisconsin–Madison, Madison, Wisconsin; [6]Radiology and Biochemistry and Molecular Genetics, University of Illinois at Chicago, Chicago, Illinois; [7]National Center for Supercomputing Applications, University of Illinois at Urbana–Champaign, Champaign, Illinois; [8]Animal Sciences, University of Illinois at Chicago, Chicago, Illinois; [9]Radiology/Interventional Radiology, University of Illinois at Chicago, Chicago, Illinois; [10]Biostatistics and Medical Informatics, University of Wisconsin–Madison, Madison, Wisconsin; [11]Medicine, Gastroenterology, and Hepatology, University of Wisconsin–Madison, Madison, Wisconsin; [12]William S. Middleton VA Medical Center, Madison, Wisconsin; [13]Surgery, University of Wisconsin–Madison, Madison, Wisconsin; and [14]Center for Biomedical Swine Research and Innovation, University of Wisconsin–Madison, Madison, Wisconsin

Current methods of staging liver fibrosis have notable limitations. We investigated the utility of PET in staging liver fibrosis by correlating liver uptake of ^{68}Ga-labeled fibroblast activation protein inhibitor (FAPI) with histology in a human-sized swine model. **Methods:** Five pigs underwent baseline ^{68}Ga-FAPI-46 (^{68}Ga-FAPI) PET/MRI and liver biopsy, followed by liver parenchymal embolization, 8 wk of oral alcohol intake, endpoint ^{68}Ga-FAPI PET/MRI, and necropsy. Regions of interest were drawn on baseline and endpoint PET images, and SUV_{mean} was recorded. At the endpoint, liver sections corresponding to regions of interest were identified and cut out. Fibrosis was histologically evaluated using a modified METAVIR score for swine liver and quantitatively using collagen proportionate area (CPA). Box-and-whisker plots and linear regression were used to correlate SUV_{mean} with METAVIR score and CPA, respectively. **Results:** Liver ^{68}Ga-FAPI uptake strongly correlated with CPA ($r = 0.89$, $P < 0.001$). ^{68}Ga-FAPI uptake was significantly and progressively higher across F2 and F3/F4 fibrosis stages, with a respective median SUV_{mean} of 2.9 (interquartile range [IQR], 2.7–3.8) and 7.6 (IQR, 6.7–10.2) ($P < 0.001$). There was no significant difference between ^{68}Ga-FAPI uptake of baseline liver and endpoint liver sections staged as F0/F1, with a respective median SUV_{mean} of 1.7 (IQR, 1.3–2.0) and 1.7 (IQR, 1.5–1.8) ($P = 0.338$). **Conclusion:** The strong correlation between liver ^{68}Ga-FAPI uptake and the histologic stage of liver fibrosis suggests that ^{68}Ga-FAPI PET can play an impactful role in noninvasive staging of liver fibrosis, pending validation in patients.

Key Words: fibroblast activation protein inhibitor; liver fibrosis; PET; MRI; swine

Liver fibrosis is the consequence of chronic liver injury of any etiology that affects 1.5 billion people worldwide (1,2). End-stage liver fibrosis (i.e., cirrhosis) is the global leading cause of liver-disease–related deaths and the most important risk factor for developing liver cancer (1). Fibrosis is the only histologic feature that predicts long-term outcomes, and serial assessments of fibrosis are of key prognostic importance in patient outcomes and assessing treatment response (3). Although liver transplant remains the only available cure for decompensated end-stage liver fibrosis, earlier stages of liver injury and fibrosis are treatable and reversible (4,5).

Current methods of assessing liver fibrosis have notable limitations. Laboratory markers are unreliable (6,7), and liver biopsy (the current gold standard) carries morbidity and mortality risks and is prone to undersampling and variability in sampling and interpretation (8–13). MR elastography is the best validated noninvasive tool and estimates liver stiffness as a surrogate for the histologic fibrosis stage (14–18). MR elastography has lower sensitivity for detection of lower stages of fibrosis, can be nondiagnostic because of liver iron overload or operator error, and cannot differentiate fibrosis from concurrent liver inflammation, as both processes increase liver stiffness (18–20). Hence, there remains a clear unmet need for a noninvasive, quantitative, and accurate tool for staging liver fibrosis.

Fibroblast activation protein (FAP) is a cell surface peptidase expressed in disease processes with matrix remodeling, such as by the fibrogenic liver stellate cells (21,22). Radiolabeled FAP inhibitors (FAPIs) have been used with PET to target FAP in vivo as an imaging tool (23,24). Advantages of PET include quantitative evaluation of radiotracer uptake by SUV and relatively operator-independent, simple whole-liver imaging. Hence, the goal of this study was to prospectively investigate the correlation between liver ^{68}Ga-FAPI-46 (^{68}Ga-FAPI) uptake on PET and the gold standard histologic stage of liver fibrosis in a human-sized swine model of alcohol-induced liver fibrosis.

MATERIALS AND METHODS

This study was conducted under protocols approved by the local Institutional Animal Care and Use Committee in accordance with
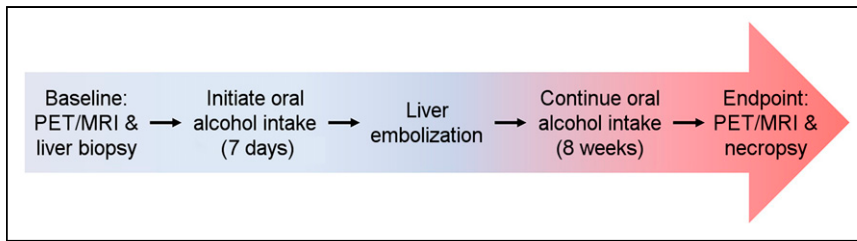
FIGURE 1. Study overview: after baseline PET/MRI, animals underwent period of gradual increase in oral alcohol intake, followed by liver parenchymal transarterial embolization. After 8 wk of oral alcohol intake, they underwent endpoint imaging followed by necropsy and tissue analysis.

published guidelines of the National Institutes of Health and U.S. Department of Agriculture. Figure 1 summarizes the study design. The swine model used in this study has been demonstrated to successfully achieve liver fibrosis (25,26) and is detailed in the supplemental materials (available at http://jnm.snmjournals.org). Five human-sized, age-matched male Wisconsin Miniature Swine™ underwent same-day PET/MRI and core-needle liver biopsy to establish baseline histologic and imaging characteristics of the liver. Increasing volumes of ethanol were then added to their daily diets over a 7-d period, followed by transarterial liver embolization with an emulsion of ethanol and ethiodized oil. The animals continued oral alcohol intake for 8 more weeks, after which they underwent endpoint PET/MRI and necropsy.

Imaging

Images were acquired under general anesthesia in the supine position on a whole-body PET/MRI scanner (Signa PET/MR; GE Healthcare). Continuous dynamic PET data of the liver were acquired for 92 min; ^{68}Ga-FAPI was administered intravenously 1 min after the initiation of data acquisitions. The average dose was 4.3 MBq (range, 3.5–4.6 MBq) per kilogram of body weight. Attenuation-corrected dynamic PET images were reconstructed with 15 s/frame for the first 5 min and 3 min/frame for the rest of the acquisition. An additional static image was generated at 60 min after radiotracer injection (using PET data at 60–69 min). Images were reviewed and analyzed by a dual board-certified nuclear medicine physician/radiologist with fellowship training in abdominal imaging and nuclear medicine, using MIM Encore (R), version 7.1.2 (MIM Software Inc.). Image analysis was performed before histologic tissue assessment to minimize bias.

Baseline Image Analysis

Circular regions of interest (ROIs) were placed on the liver parenchyma on MRI, avoiding major vessels: 1 in the right lobe and 1 in the left lobe, with a minimum diameter of 1.5 cm. Each ROI was propagated across 1 slice cranially and 1 slice caudally, yielding a cylindric ROI with a minimum volume of 4 cm^3. To minimize bias, ROIs were propagated directly by the software into both dynamic and static PET images. The SUV$_{mean}$ for each ROI was recorded, yielding 10 data points at baseline (2 per animal).

Endpoint Image Analysis

Because of the heterogeneous nature of the fibrosis achieved by this model (dictated by preferential liver arterial flow carrying different volumes of embolic emulsion to different liver regions), 4 ROIs for each animal were placed on the static PET images. To achieve

adequate assessment across the uptake spectrum, 2 of the ROIs were placed on the most avid areas and 2 on relatively less avid areas. Second, ROIs were placed in areas that could be localized on harvested livers using anatomic landmarks (e.g., gallbladder fossa and major vessels). This approach yielded 20 data points at the endpoint (4 per animal).

Tissue Procurement and Histology

Baseline core samples were obtained from each liver lobe. Livers were harvested at the endpoint, and lobar surfaces were marked with ink to preserve the landmarks needed for imaging–histology colocalization. Livers were sectioned using a bread-loafing technique in the axial plane to resemble the slices on PET/MRI, and all slices were fixed in formalin. Using anatomic landmarks, liver areas corresponding to the ROIs on endpoint images were identified, and wedge sections from these regions were cut out.

All tissue samples were processed with Masson trichrome stain, picrosirius red stain, and anti-FAP immunohistochemistry. Histologic review and analysis were performed by a board-certified fellowship-trained hepatobiliary pathologist, unaware of the imaging results and the time points of tissue procurement. Two histologic standards were used as references: METAVIR fibrosis score (27,28) and collagen proportionate area (CPA) (29–35). The METAVIR score is an ordinal 5-point scale (F0–F4); in humans, F0 is absence of fibrosis and F4 is end-stage fibrosis/cirrhosis. Given that normal swine liver has thin, organized bands of fibrosis, for the purposes of this study F0 and F1 were grouped into 1 category (F0/F1) and assigned to normal swine liver (Fig. 2). CPA is the proportion of collagen deposition area relative to the total tissue area (reported in %) on picrosirius red–stained slides. CPA analysis was performed only for endpoint wedge sections and not for baseline tissues, because of the relatively small amount of tissue procured through core needle biopsy at baseline.

Statistical Analysis

Liver FAPI uptake time–activity curves were generated by plotting the pooled ROI SUV$_{mean}$ against time for different stages of fibrosis. Box-and-whisker plots were generated to compare liver ^{68}Ga-FAPI uptake and CPA across different histologic stages of liver fibrosis,

FIGURE 2. Modified METAVIR score to stage swine liver fibrosis: because of presence of thin bands of fibrosis in normal swine liver and absence of this finding in normal human liver, METAVIR score used for staging human liver fibrosis was modified, such that a new stage (F0/F1) corresponds to normal swine liver with expected thin bands of fibrosis. Representative Masson trichrome–stained histologic slides of swine liver demonstrate extent of fibrosis at each stage.
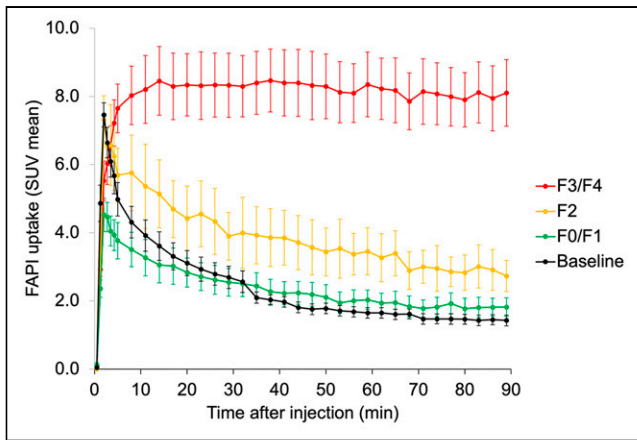
FIGURE 3. Pooled-data time–activity curves demonstrate similar pattern of ^{68}Ga-FAPI uptake by both normal liver at baseline and F0/F1 sections at endpoint. Conversely, there is incremental increase in delayed ^{68}Ga-FAPI uptake by liver sections histologically staged as F2 and as F3/F4 ($P < 0.001$).

using the Kruskal–Wallis rank sum test. Linear regression was used to correlate liver ^{68}Ga-FAPI uptake with CPA, applying the Pearson correlation coefficient. To account for the correlation among repeated measurements and their nonmonotone change over time, a linear mixed-effects model was used with pig- and ROI-specific random effects and a piecewise linear time trend. Time–activity curves were compared using an F test on longitudinal measurements assuming normally distributed errors. P values of less than 0.05 were considered statistically significant. A post hoc power analysis for testing F2 versus F0/F1, and F3/F4 versus F0/F1, under the current sample size was performed.

RESULTS

All animals completed the study procedures. Baseline PET imaging of animal 2 was terminated at 69 min after injection, when the animal had to be removed from the scanner to reestablish the airway and ensure animal safety. For animal 3, PET data at 37–42 min were discarded because of a shift in the animal's position inside the scanner during that period, but imaging was completed successfully. Time–activity curves demonstrated incrementally higher delayed ^{68}Ga-FAPI uptake in stage F2 and F3/F4 sections ($P < 0.001$, Fig. 3). Uptake was stabilized at 60 min, the time point at which the static images were generated for purposes of quantitative analysis and imaging–histology correlation.

Figure 4 is an example of imaging–histology correlation in the same animal at baseline and at the endpoint; the embolized region of the liver demonstrated fibrosis with avid ^{68}Ga-FAPI uptake. Table 1 summarizes the ^{68}Ga-FAPI uptake and the corresponding METAVIR score and CPA for all liver sections. All baseline liver samples were normal (stage F0/F1). At the endpoint, of the total 20 liver sections, 9 were staged as F0/F1, 3 as F2, 1 as F3, and 7 as F4. Given that only 1 specimen was staged as

F3, it was grouped with the F4 specimens (i.e., group F3/F4) to provide for a meaningful quantitative analysis.

There was a strong linear correlation between liver ^{68}Ga-FAPI uptake and histologic CPA ($r = 0.89$, $P < 0.001$, Fig. 5A). There was no significant difference between the uptake of baseline liver and endpoint liver sections staged as F0/F1, with a respective median SUV_{mean} of 1.7 (interquartile range [IQR], 1.3–2.0) and 1.7 (IQR, 1.5–1.8) ($P = 0.338$). Conversely, ^{68}Ga-FAPI uptake was significantly higher across the F2 and F3/F4 stages and directly correlated with the histologic fibrosis stage, with a respective median SUV_{mean} of 2.9 (IQR, 2.7–3.8) and 7.6 (IQR, 6.7–10.2) ($P < 0.001$, Fig. 5B). There was also a significant increase in CPA across fibrosis stages, with a median CPA of 14% (IQR, 13%–16%) for F0/F1, 33% (IQR, 31%–36%) for F2, and 49% (IQR, 47%–61%) for F3/F4 (all $P < 0.001$, Fig. 5C). The post hoc power of testing F2 versus F0/F1, and F3/F4 versus F0/F1, under the current sample size was calculated as, respectively, 44% and 99.99%.

DISCUSSION

We demonstrated that liver ^{68}Ga-FAPI uptake strongly correlates with 2 accepted histologic metrics of liver fibrosis across the observed fibrosis stages in a human-sized swine model. Other molecular imaging agents have also been investigated for this purpose. Increased liver uptake of ^{18}F-alfatide in more advanced stages of fibrosis in a mouse model has been reported (36). However, normal liver uptake of ^{18}F-alfatide appears to be substantial enough to render this agent suboptimal for discerning lower stages of fibrosis (36,37). A study of ^{11}C-aminoglycerol PET in a rat model demonstrated an inverse correlation between liver radiotracer uptake and fibrosis stage. Key limitations of this approach include a very short radiotracer half-life and overlap of uptake intensity between fibrosis stages (38). Last, ^{18}F-FDG PET plays only a limited role in evaluation of liver fibrosis, mainly due to altered liver glucose metabolism in the setting of chronic liver disease (39).

^{68}Ga-FAPI PET can offer several key potential advantages for evaluation of liver fibrosis. In our human-sized swine model, ^{68}Ga-FAPI differentiated between various stages of disease.
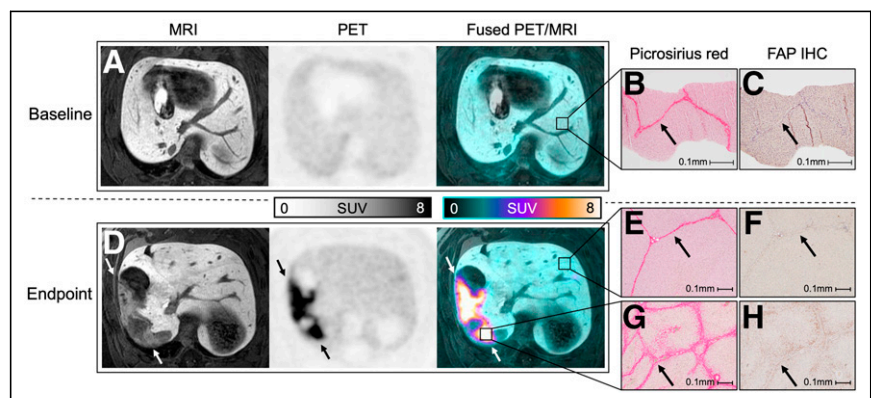

FIGURE 4. Imaging–histology correlation at baseline and endpoint. (A) Baseline axial PET/MR images of animal 5 demonstrate homogeneous liver parenchyma and mild ^{68}Ga-FAPI uptake. (B and C) Core biopsy of left liver lobe (at ×100 magnification) demonstrates expected thin bands of fibrosis (B, arrow), with very faint staining on FAP immunohistochemistry (C, arrow). (D) At endpoint, geographic region in right lobe demonstrates hypoenhancement on MRI and increased ^{68}Ga-FAPI uptake (arrows). (E–H) Liver sections obtained from avid (abnormal) and nonavid (normal/spared) regions (at ×40 magnification) demonstrate expected thin bands of fibrosis in normal/spared region (E, arrow), with minimal staining on FAP immunohistochemistry (F, arrow), and, conversely, thickened bridging bands of fibrosis in abnormal region (G, arrow), with positive staining on FAP immunohistochemistry (H, arrow). IHC = immunohistochemistry.

TABLE 1
Summary of Liver ^{68}Ga-FAPI Uptake on PET and Histologic Analysis of Liver Tissue Core Biopsy and Wedge Sections in All Subjects at Baseline and at Endpoint

Animal no.	Liver tissue	^{68}Ga-FAPI SUV$_{mean}$	METAVIR score	CPA* (%)
1	Baseline core (left lobe)	1.8	F0/F1	—
	Baseline core (right lobe)	1.6	F0/F1	—
	Endpoint section 1	7.0	F4	50
	Endpoint section 2	1.5	F0/F1	15
	Endpoint section 3	5.8	F4	49
	Endpoint section 4	1.5	F0/F1	14
2	Baseline core (left lobe)	2.4	F0/F1	—
	Baseline core (right lobe)	2.0	F0/F1	—
	Endpoint section 1	2.5	F2	39
	Endpoint section 2	2.9	F2	33
	Endpoint section 3	1.7	F0/F1	9
	Endpoint section 4	1.5	F0/F1	12
3	Baseline core (left lobe)	2.2	F0/F1	—
	Baseline core (right lobe)	1.9	F0/F1	—
	Endpoint section 1	6.9	F4	40
	Endpoint section 2	2.1	F0/F1	22
	Endpoint section 3	1.8	F0/F1	13
	Endpoint section 4	4.9	F3	49
4	Baseline core (left lobe)	0.8	F0/F1	—
	Baseline core (right lobe)	1.2	F0/F1	—
	Endpoint section 1	4.7	F2	29
	Endpoint section 2	10.6	F4	77
	Endpoint section 3	4.5	F0/F1	16
	Endpoint section 4	12.6	F4	67
5	Baseline core (left lobe)	1.3	F0/F1	—
	Baseline core (right lobe)	1.3	F0/F1	—
	Endpoint section 1	8.3	F4	59
	Endpoint section 2	10.1	F4	44
	Endpoint section 3	1.6	F0/F1	13
	Endpoint section 4	1.7	F0/F1	18

*CPA was not calculated at baseline because only core biopsies were obtained.

Furthermore, considering minimal uptake in normal human liver (40,41), ^{68}Ga-FAPI may detect early changes of fibrosis, which would be advantageous over elastography. Additional advantages of ^{68}Ga-FAPI PET over elastography would be whole-liver evaluation, minimal opportunity for operator error, and robustness against factors that contribute to or confound liver stiffness measurement, most notably concurrent liver inflammation (16). Although a more novel 3-dimensional MR elastography technique has demonstrated potential to address this limitation (42), this concept has not been validated in clinical practice. However, considering the ability of MRI to accurately assess several key aspects of diffuse liver disease, such as fat, iron, and stiffness (43,44), it is likely that combined ^{68}Ga-FAPI PET and MRI/MR elastography may provide complementary information to paint a more complete picture of the state of liver disease. Potential disadvantages of ^{68}Ga-FAPI PET include radiation exposure

and radiotracer availability. However, human dosimetry of ^{68}Ga-FAPI has demonstrated a whole-body exposure that is similar to that of ^{18}F-FDG (41,45). There remain challenges and unknowns that should be addressed as part of further validation of the utility of ^{68}Ga-FAPI PET in assessment of liver fibrosis. Although ^{68}Ga-FAPI uptake directly correlated with the stage of fibrosis in the presented model, this correlation was observed in the setting of active fibrosis in which the animals continued alcohol intake daily. Whether this observation is reproducible in other chronic disease processes, such as in viral hepatitis and nonalcoholic steatohepatitis, is of significant scientific and clinical relevance and requires further validation.

This study had some limitations. Although the sample size was small, a post hoc power analysis demonstrated its adequacy, which was also on a par with a previous report (46). Furthermore, this model generated patchy or geographic areas of fibrotic and normal
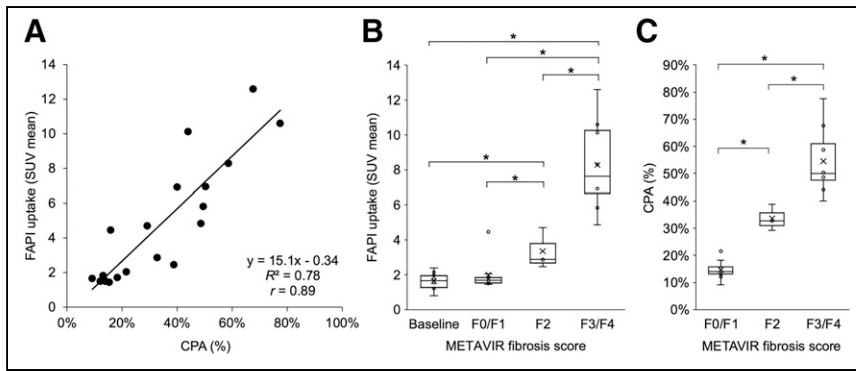
FIGURE 5. (A) Linear regression demonstrates strong correlation between liver ^{68}Ga-FAPI uptake and histologic CPA ($r = 0.89$). (B) Box-and-whisker plot of liver ^{68}Ga-FAPI uptake for METAVIR fibrosis stage groups demonstrates no significant difference between baseline liver uptake and endpoint uptake in liver sections staged as F0/F1 ($P = 0.338$); however, there is significant and incrementally higher ^{68}Ga-FAPI uptake across F2 and F3/F4 stages, with minimal overlap between different stages ($P < 0.001$). (C) Box-and-whisker plot of histologic CPA for each METAVIR fibrosis stage group at endpoint, demonstrating significant and incrementally increased CPA with increasing fibrosis stage ($P < 0.001$). CPA was not performed for baseline tissues because relatively small amount of tissue was procured through core needle biopsy at baseline. *Statistical significance.

liver, a pattern that is different from the pattern of disease in humans. However, this feature allowed for an internal negative control. Another limitation of a swine model is the presence of thin fibrotic bands in normal liver, explaining ^{68}Ga-FAPI uptake by normal liver. Hence, the potential of ^{68}Ga-FAPI PET to differentiate between F0 and F1 stages of disease would have to be investigated in human subjects. Our data yielded only 1 specimen with F3 liver fibrosis; hence, we were unable to evaluate the ability of ^{68}Ga-FAPI PET to discern between F3 and F4 stages. Although worth investigating, the significance of this limitation is unknown, as often in clinical practice or in the research setting, F0 and F1 stages as well as F3 and F4 stages are grouped for treatment or prognostic purposes. Last, despite the careful approach to achieve accurate and unbiased imaging–histology correlation through masking and using only anatomic landmarks to obtain tissue samples that correspond to ROIs, sampling error or variability cannot be completely eliminated. This variability and limitation are not unique to this study and are also present in current clinical practice, as well as in nearly all studies that have evaluated liver fibrosis. We anticipate that once ^{68}Ga-FAPI PET for assessment of liver fibrosis is further investigated and potentially validated in humans, it will largely overcome the aforementioned limitations of the current techniques and enhance our ability to understand disease progression and evolution among those with chronic liver disease.

CONCLUSION

The strong correlation between liver ^{68}Ga-FAPI uptake and the histologic stage of liver fibrosis suggests that ^{68}Ga-FAPI PET can play an impactful role in noninvasive staging of liver fibrosis, pending validation in patients. This technique can be used not only in the clinical setting but also for clinical trials (e.g., drug development) or for validation of other novel techniques for assessment of diffuse liver disease.

DISCLOSURE

KEY POINTS

QUESTION: Is there potential for ^{68}Ga-FAPI PET in staging liver fibrosis?

PERTINENT FINDINGS: This animal study demonstrated a direct correlation between quantitative liver ^{68}Ga-FAPI uptake on PET and both histologic measures of liver fibrosis, that is, the ordinal METAVIR score and the quantitative CPA.

IMPLICATIONS FOR PATIENT CARE: Pending further validation in patients, ^{68}Ga-FAPI PET is a promising tool for noninvasive liver fibrosis staging.

REFERENCES

1. GBD 2017 Cirrhosis Collaborators. The global, regional, and national burden of cirrhosis by cause in 195 countries and territories, 1990-2017: a systematic analysis for the Global Burden of Disease Study 2017. *Lancet Gastroenterol Hepatol.* 2020;5:245–266.
2. Ge PS, Runyon BA. Treatment of patients with cirrhosis. *N Engl J Med.* 2016;375:767–777.
3. Angulo P, Kleiner DE, Dam-Larsen S, et al. Liver fibrosis, but no other histologic features, is associated with long-term outcomes of patients with nonalcoholic fatty liver disease. *Gastroenterology.* 2015;149:389–397.e10.
4. D'Ambrosio R, Aghemo A, Rumi MG, et al. A morphometric and immunohistochemical study to assess the benefit of a sustained virological response in hepatitis C virus patients with cirrhosis. *Hepatology.* 2012;56:532–543.
5. Marcellin P, Gane E, Buti M, et al. Regression of cirrhosis during treatment with tenofovir disoproxil fumarate for chronic hepatitis B: a 5-year open-label follow-up study. *Lancet.* 2013;381:468–475.
6. Alberti A, Noventa F, Benvegnu L, Boccato S, Gatta A. Prevalence of liver disease in a population of asymptomatic persons with hepatitis C virus infection. *Ann Intern Med.* 2002;137:961–964.
7. Harris R, Harman DJ, Card TR, Aithal GP, Guha IN. Prevalence of clinically significant liver disease within the general population, as defined by non-invasive

markers of liver fibrosis: a systematic review. *Lancet Gastroenterol Hepatol.* 2017; 2:288–297.

8. Sumida Y. Limitations of liver biopsy and non-invasive diagnostic tests for the diagnosis of nonalcoholic fatty liver disease/nonalcoholic steatohepatitis. *World J Gastroenterol.* 2014;20:475–485.

9. Rousselet M-C, Michalak S, Dupré F, et al. Sources of variability in histological scoring of chronic viral hepatitis. *Hepatology.* 2005;41:257–264.

10. Goldin RD, Goldin JG, Burt AD, et al. Intra-observer variation in the histopathological assessment of chronic viral hepatitis. *J Hepatol.* 1996;25:649–654.

11. Maharaj B, Maharaj RJ, Leary WP, et al. Sampling variability and its influence on the diagnostic yield of percutaneous needle biopsy of the liver. *Lancet.* 1986;1: 523–525.

12. Regev A, Berho M, Jeffers LJ, et al. Sampling error and intraobserver variation in liver biopsy in patients with chronic HCV infection. *Am J Gastroenterol.* 2002;97: 2614–2618.

13. Bravo AA, Sheth SG, Chopra S. Liver biopsy. *N Engl J Med.* 2001;344:495–500.

14. Singh S, Venkatesh SK, Wang Z, et al. Diagnostic performance of magnetic resonance elastography in staging liver fibrosis: a systematic review and meta-analysis of individual participant data. *Clin Gastroenterol Hepatol.* 2015;13:440–451.e6.

15. Yin M, Woollard J, Wang X, et al. Quantitative assessment of hepatic fibrosis in an animal model with magnetic resonance elastography. *Magn Reson Med.* 2007; 58:346–353.

16. Tang A, Cloutier G, Szeverenyi NM, Sirlin CB. Ultrasound elastography and MR elastography for assessing liver fibrosis: part 2, diagnostic performance, confounders, and future directions. *AJR.* 2015;205:33–40.

17. Wang QB, Zhu H, Liu HL, Zhang B. Performance of magnetic resonance elastography and diffusion-weighted imaging for the staging of hepatic fibrosis: a meta-analysis. *Hepatology.* 2012;56:239–247.

18. Yin M, Glaser KJ, Talwalkar JA, Chen J, Manduca A, Ehman RL. Hepatic MR elastography: clinical performance in a series of 1377 consecutive examinations. *Radiology.* 2016;278:114–124.

19. Chen J, Talwalkar JA, Yin M, Glaser KJ, Sanderson SO, Ehman RL. Early detection of nonalcoholic steatohepatitis in patients with nonalcoholic fatty liver disease by using MR elastography. *Radiology.* 2011;259:749–756.

20. Salameh N, Larrat B, Abarca-Quinones J, et al. Early detection of steatohepatitis in fatty rat liver by using MR elastography. *Radiology.* 2009;253:90–97.

21. Levy MT, McCaughan GW, Abbott CA, et al. Fibroblast activation protein: a cell surface dipeptidyl peptidase and gelatinase expressed by stellate cells at the tissue remodelling interface in human cirrhosis. *Hepatology.* 1999;29:1768–1778.

22. Uitte de Willige S, Malfliet JJMC, Janssen HLA, Leebeek FWG, Rijken DC. Increased N-terminal cleavage of alpha-2-antiplasmin in patients with liver cirrhosis. *J Thromb Haemost.* 2013;11:2029–2036.

23. Shi X, Xing H, Yang X, et al. Fibroblast imaging of hepatic carcinoma with ^{68}Ga-FAPI-04 PET/CT: a pilot study in patients with suspected hepatic nodules. *Eur J Nucl Med Mol Imaging.* 2021;48:196–203.

24. Loktev A, Lindner T, Mier W, et al. A tumor-imaging method targeting cancer-associated fibroblasts. *J Nucl Med.* 2018;59:1423–1429.

25. Gaba RC, Mendoza-Elias N, Regan DP, et al. Characterization of an inducible alcoholic liver fibrosis model for hepatocellular carcinoma investigation in a transgenic porcine tumorigenic platform. *J Vasc Interv Radiol.* 2018;29:1194–1202.e1.

26. Avritscher R, Wright KC, Javadi S, et al. Development of a large animal model of cirrhosis and portal hypertension using hepatic transarterial embolization: a study in swine. *J Vasc Interv Radiol.* 2011;22:1329–1334.

27. The French METAVIR Cooperative Study Group. Intraobserver and interobserver variations in liver biopsy interpretation in patients with chronic hepatitis C. *Hepatology.* 1994;20:15–20.

28. Bedossa P, Poynard T. An algorithm for the grading of activity in chronic hepatitis C. *Hepatology.* 1996;24:289–293.

29. Buzzetti E, Hall A, Ekstedt M, et al. Collagen proportionate area is an independent predictor of long-term outcome in patients with non-alcoholic fatty liver disease. *Aliment Pharmacol Ther.* 2019;49:1214–1222.

30. Tsochatzis E, Bruno S, Isgro G, et al. Collagen proportionate area is superior to other histological methods for sub-classifying cirrhosis and determining prognosis. *J Hepatol.* 2014;60:948–954.

31. Calvaruso V, Dhillon AP, Tsochatzis E, et al. Liver collagen proportionate area predicts decompensation in patients with recurrent hepatitis C virus cirrhosis after liver transplantation. *J Gastroenterol Hepatol.* 2012;27:1227–1232.

32. Manousou P, Burroughs AK, Tsochatzis E, et al. Digital image analysis of collagen assessment of progression of fibrosis in recurrent HCV after liver transplantation. *J Hepatol.* 2013;58:962–968.

33. Calvaruso V, Burroughs AK, Standish R, et al. Computer-assisted image analysis of liver collagen: relationship to Ishak scoring and hepatic venous pressure gradient. *Hepatology.* 2009;49:1236–1244.

34. Xie SB, Ma C, Lin CS, Zhang Y, Zhu JY, Ke WM. Collagen proportionate area of liver tissue determined by digital image analysis in patients with HBV-related decompensated cirrhosis. *Hepatobiliary Pancreat Dis Int.* 2011;10:497–501.

35. Isgro G, Calvaruso V, Andreana L, et al. The relationship between transient elastography and histological collagen proportionate area for assessing fibrosis in chronic viral hepatitis. *J Gastroenterol.* 2013;48:921–929.

36. Shao T, Chen Z, Belov V, et al. [^{18}F]-Alfatide PET imaging of integrin αvβ3 for the non-invasive quantification of liver fibrosis. *J Hepatol.* 2020;73:161–169.

37. Wu J, Wang S, Zhang X, et al. ^{18}F-Alfatide II PET/CT for identification of breast cancer: a preliminary clinical study. *J Nucl Med.* 2018;59:1809–1816.

38. Chen X, Zhang X, Du M, et al. In vivo preclinical PET/CT imaging of carbon-11-labeled aminoglycerol probe for the diagnosis of liver fibrosis. *Ann Nucl Med.* 2019;33:806–812.

39. Verloh N, Einspieler I, Utpatel K, et al. In vivo confirmation of altered hepatic glucose metabolism in patients with liver fibrosis/cirrhosis by ^{18}F-FDG PET/CT. *EJNMMI Res.* 2018;8:98.

40. Kratochwil C, Flechsig P, Lindner T, et al. ^{68}Ga-FAPI PET/CT: tracer uptake in 28 different kinds of cancer. *J Nucl Med.* 2019;60:801–805.

41. Giesel FL, Kratochwil C, Lindner T, et al. ^{68}Ga-FAPI PET/CT: biodistribution and preliminary dosimetry estimate of 2 DOTA-containing FAP-targeting agents in patients with various cancers. *J Nucl Med.* 2019;60:386–392.

42. Shi Y, Qi YF, Lan GY, et al. Three-dimensional MR elastography depicts liver inflammation, fibrosis, and portal hypertension in chronic hepatitis B or C. *Radiology.* 2021;301:154–162.

43. Yokoo T, Serai SD, Pirasteh A, et al. Linearity, bias, and precision of hepatic proton density fat fraction measurements by using MR imaging: a meta-analysis. *Radiology.* 2018;286:486–498.

44. Wood JC, Enriquez C, Ghugre N, et al. MRI R2 and R2* mapping accurately estimates hepatic iron concentration in transfusion-dependent thalassemia and sickle cell disease patients. *Blood.* 2005;106:1460–1465.

45. Johansson L, Mattsson S, Nosslin B, Leide-Svegborn S. Effective dose from radio-pharmaceuticals. *Eur J Nucl Med.* 1992;19:933–938.

46. Yin M, Glaser KJ, Manduca A, et al. Distinguishing between hepatic inflammation and fibrosis with MR elastography. *Radiology.* 2017;284:694–705.